Charge Properties of TiO2 Nanotubes in NaNO3 Aqueous Solution

Mario Špadina, Simon Gourdin-Bertin, Goran Dražić, Atiđa Selmani, Jean-François Dufrêche, Klemen Bohinc

ACS APPLIED MATERIALS & INTERFACES

Research Article

Cite This: ACS Appl. Mater. Interfaces XXXX, XXX, XXX−XXX

www.acsami.org

Charge Properties of TiO_2 Nanotubes in $NaNO_3$ Aqueous Solution

Mario Špadina,[†] Simon Gourdin-Bertin,[†] Goran Dražić,[‡] Atiđa Selmani,[§] Jean-François Dufrêche,[†] and Klemen Bohinc*[,∥]

[†]Institut de Chimie Séparative de Marcoule (ICSM), UMR 5257, CEA, Université de Montpellier, CNRS, ENSCM, BP 17171, F-30207 Bagnols-sur-Ceze, France

[‡]Laboratory for Materials Chemistry, National Institute of Chemistry, SI-1000 Ljubljana, Slovenia

[§]Division of Physical Chemistry, Ruđer Boškovic Institute, 10000 Zagreb, Croatia

[∥]Faculty of Health Sciences, University of Ljubljana, Zdravstvena 5, SI-1000 Ljubljana, Slovenia

Supporting Information

ABSTRACT: Charging of material surfaces in aqueous electrolyte solutions is one of the most important processes in the interactions between biomaterials and surrounding tissue. Other than a biomaterial, titania nanotubes (TiO_2 NTs) represent a versatile material for numerous applications such as heavy metal adsorption or photocatalysis. In this article, the surface charge properties of titania NTs in $NaNO_3$ solution were investigated through electrophoretic mobility and polyelectrolyte colloid titration measuring techniques. In addition, we used high-resolution transmission electron microscopy imaging to determine the morphology of TiO_2 NTs. A theoretical model based on the classical density functional theory coupled with the charge regulation method in terms of mass action law was developed to understand the experimental data and to provide insights into charge properties at different physical conditions, namely, pH and $NaNO_3$ concentration. Two intrinsic protonation constants and surface site density have been obtained. The electrostatic properties of the system in terms of electrostatic potentials and ion distributions were calculated and discussed for various pH values. The model can quantitatively describe the titration curve as a function of pH for higher bulk salt concentrations and the difference in the equilibrium amount of charges between the inner and outer surfaces of TiO_2 NTs. Calculated counterion (NO_3^-) distributions show a pronounced decrease of NO_3^- ions for high bulk pH (both inside and outside TiO_2 NT) because of the strong electric field. With the decrease of bulk pH or the increase of the salt concentration, NO_3^- is able to accumulate near the TiO_2 NTs surfaces.

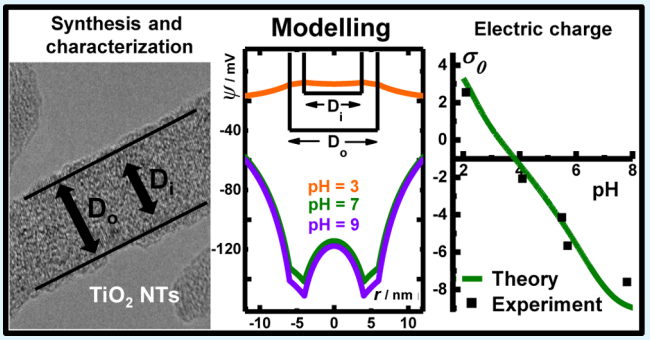

KEYWORDS: *HR-TEM, polyelectrolyte, mobility, charge, Poisson−Boltzmann, adsorption, electrostatic, potential, distribution*

1. INTRODUCTION

Specific and often enhanced properties of TiO_2 nanomaterials make them suitable for various applications such as adsorbents for different organic molecules and heavy metal ions.[1,2] Furthermore, TiO_2 nanomaterials can be used for degradation of environmental pollutants by exploiting their photocatalytic properties or even as carriers of various matters in a nanomedical application.[3−6] The efficiency of these possible applications is governed by morphology factors such as the crystal structure, size distribution, porosity, surface area, and so forth. Almost all applications are governed by processes in aqueous electrolyte solutions. Therefore, it is understandable that the TiO_2 nanomaterial charge properties have an important impact on the efficiency of those applications.

Particularly interesting nanomaterials are TiO_2 nanotubes (shorten TiO_2 NTs). The TiO_2 NTs are tubular multilayered hollow nanomaterials which are usually obtained by hydrothermal synthesis.[7] The crystal structure of TiO_2 NTs varies with different synthesis conditions and starting materials used.[8]

The transmission electron microscopy has been employed to get insight into the differences between the inner and the outer TiO_2 NTs radius. In NT morphology besides the size also crystallinity, a number of walls, defects, and functionalizations can be investigated with various imaging, diffraction, and spectroscopy techniques.[9]

Lately, the TiO_2 NT charge properties in aqueous electrolyte solutions have been investigated from both experimental and theoretical aspects. Rather large discrepancies were found between the calculated and measured data.[10] Various methods have been used for the determination of surface charge density such as potentiometric acid−base and mass titration and

Received: December 9, 2017
Accepted: March 16, 2018

DOI: 10.1021/acsami.7b18737
ACS Appl. Mater. Interfaces XXXX, XXX, XXX−XXX

estimation of the point of zero charge from electrokinetic measurements.[11−13] Besides the mentioned techniques, the polyelectrolyte titration with streaming potential measurement (colloid titration) was recognized as a method of choice for the surface charge determination of various types of colloid particles that differ in size and shape, including TiO_2 NTs.[3,14,15]

The advantage of the polyelectrolyte titration over conventional methods lies in the simplicity of conducting the experiment which is monitoring a response of the streaming potential as a function of the titrant volume added. The method is especially accurate at low salt concentrations.[16] A standardized aqueous solution of a strong polyelectrolyte serves as titrant. From the polyelectrolyte titration curve, the point of zero charge can be obtained. The end point observed in the polyelectrolyte titration curve corresponds to compensation of a total charge of investigated particles. Regardless of the structure of the titrated particle, the polyelectrolyte binds to the surface and compensates the charge. Binding of the titrant is governed by strong electrostatic forces between the particle surface and monomer units of the polyelectrolyte.[17]

The interpretation of the potentiometric titration or polyelectrolyte titration when applied to porous materials, such as TiO_2 NTs, is rather difficult. Where does the compensated charge come from? Is it possible to state what the ratio of charge on the inner and outer TiO_2 NT surface is? To answer these questions, we turn to a theoretical approach.

To understand the behavior of charged colloids in aqueous electrolyte solution, the Poisson−Boltzmann theory is often used because in low salt conditions, it provides satisfying explanations.[18] The Poisson−Boltzmann theory is often coupled with the charge regulation method to explain various phenomena in colloidal chemistry.[19] Advancements toward more realistic descriptions of colloidal systems include interactions between dissimilar surfaces, rod-like polyions, mobile surface groups, and even the interactions between soft multilayered particles.[20−23] Advanced classical density functional theory, hypernetted-chain integral equation theory, molecular dynamics, and Monte Carlo simulations made considerable progress about the description of ion density profiles inside confined media and about the evaluation of surface charge of porous materials.[24−29]

Yet, to our knowledge, there is no model that can quantitatively describe the charge difference between the inner and outer surfaces of porous materials. Moreover, it is not clear where the adsorption of ions takes place. As stated before, we turn to address such problems on the TiO_2 NT system which we consider to be one of the simplest examples of such a group of materials.

Within this work, we aim to show the whole experimental procedure, from the known and well-established synthesis of TiO_2 NTs and high-resolution transmission electron microscopy (HR-TEM) characterization to charge determination experiments. From morphology data, we will determine the distribution of TiO_2 NT inner and outer radii. The mobility measurements will provide qualitative description, whereas the polyelectrolyte titration in the particle charge detector will provide a quantitative description of the TiO_2 NT charge through the pH region between 2 and 10.

Also, we will show a step-by-step development of a simple but predictive theoretical model of a charged TiO_2 NT immersed in the aqueous $NaNO_3$ solution. With the model, we will fit the experimental data of the polyelectrolyte titration to obtain protonation constants and surface site density. The fitting process and the interpretation of the experimental data will be discussed.

The last part of this work is dedicated to theoretical predictions of the charge properties of TiO_2 NTs for various physical conditions such as pH and reservoir salt concentrations. We will also consider the charge differences between the inner and outer surfaces of the TiO_2 NTs as well as the extent of the Donnan effect.

2. THEORY

The TiO_2 NTs are modeled as infinitely long cylinders so the electric field edge effects are neglected. The inner cylinder radius is R_i = 4 nm, and the outer radius is R_o = 6 nm (Figure 2b, inset). Both the inner and outer cylinder surfaces are in contact with an aqueous solution of a univalent electrolyte. The origin of a cylindrical coordinate system is placed at the center of the cylinder with the abscissa axis being radial coordinate r and the ordinate axis being along the cylinder axis. Both the electrolyte solution and the TiO_2 layer are considered as dielectric continua with dielectric constants $\epsilon_{r,1}$ and $\epsilon_{r,2}$, where $\epsilon_{r,1}$ corresponds to electrolyte solution and $\epsilon_{r,2}$ corresponds to the solid TiO_2 layer.

The inner cylinder surface is characterized by the uniform surface charge density σ_i and the outer surface with the uniform surface charge density σ_o.

2.1. Charge Regulation. The charge of TiO_2 NTs is pH-dependent, which means that there is an equilibrium between amphoteric surface groups and ions in the solution. The surface charge density is regulated via the mass action law.[30] Figure 1 shows the schematic representation of the charging processes that take place at both TiO_2 NT surfaces. According to the experimental data, the anatase planes were identified in the sample. In the anatase phase, Ti^{4+} is coordinated in octahedra with six oxygen atoms. As a surface site, we have chosen to consider only singly coordinated sites. Using the Pauling concept to estimate bond valence points to the fact that the

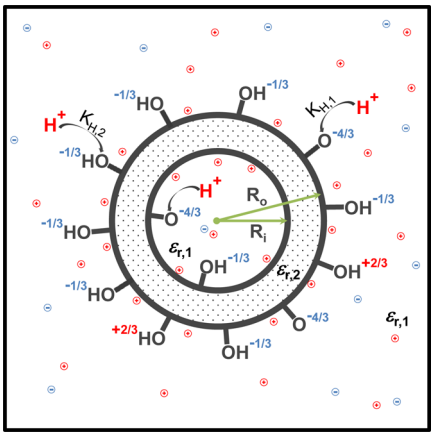

Figure 1. Schematic cross section of TiO_2 NTs. The cross section is perpendicular to the cylinder axis of symmetry. R_i and R_o correspond to the inner and outer cylinder radii, respectively. $\epsilon_{r,1}$ and $\epsilon_{r,2}$ correspond to electrolyte solution and TiO_2 layer dielectric constants, respectively. Surface groups $\equiv TiO^{-4/3}$, $\equiv TiOH^{-1/3}$, and $\equiv TiOH_2^{+2/3}$ are in equilibrium with surrounding electrolyte solution. $K_{H,1}$ and $K_{H,2}$ are surface reaction constants. Proton ions H^+ are distinguished from other ions only because of surface equilibria and autoprotolysis of water. Within the model, all ions are point-like charges.

DOI: 10.1021/acsami.7b18737
ACS Appl. Mater. Interfaces XXXX, XXX, XXX−XXX

fully deprotonated surface oxygen atom bonded to one Ti^{4+} has $-4/3e$ charge,[31,32] where e is elementary charge. For such surface groups, the following equilibrium protonation reactions are obtained[33]

$$\equiv TiO^{-4/3} + H^+ \rightleftharpoons \equiv TiOH^{-1/3} \quad (1)$$

and

$$\equiv TiOH^{-1/3} + H^+ \rightleftharpoons \equiv TiOH_2{}^{+2/3} \quad (2)$$

The two equations can be expressed through intrinsic equilibrium constants $K_{H,1}$

$$K_{H,1} = \frac{\{\equiv TiOH^{-1/3}\}}{\{\equiv TiO^{-4/3}\}[H^+]_{loc}} \quad (3)$$

and $K_{H,2}$

$$K_{H,2} = \frac{\{\equiv TiOH_2{}^{+2/3}\}}{\{\equiv TiOH^{-1/3}\}[H^+]_{loc}} \quad (4)$$

where $[H^+]_{loc}$ is local (surface) proton concentrations.[34] The influence of surface groups is taken into account indirectly through mean field approximation.[22]

The autoprotolysis of water has been taken into account to adjust the reservoir proton and hydroxide ion concentrations. The reaction

$$H_2O \rightleftharpoons H^+ + OH^- \quad (5)$$

can be written as

$$K_w = [H^+]_0[OH^-]_0 \quad (6)$$

where the subscript 0 denotes the bulk equilibrium concentrations and K_w is the autoprotolysis constant for water.[35]

Because our experimental salt concentrations are around 0.001 M while the molar concentration of surface groups is around 0.0001 M, it is safe to assume the ideality of the solution and all its species. Throughout the model, the activity coefficients γ are chosen to be 1.[36] With such a formulation, the surface site density Γ is the sum of all equilibrium surface site concentrations.[37]

$$\Gamma = \{\equiv TiO^{-4/3}\} + \{\equiv TiOH^{-1/3}\} + \{\equiv TiOH_2{}^{+2/3}\} \quad (7)$$

Combining eqs 3, 4, and 7 yields expressions for equilibrium surface concentrations of each group. The acquired expression is, in fact, typical Langmuir-like competitive adsorption equation.[38] For convenience, it is desirable to write the equilibrium surface concentrations as a product of total site density and the factor called fractional coverage f_1. The fractional coverage f_1 defines the ratio of the particular charged group in the total number of sites on the plane for a given conditions T, pH, and so forth

$$f_1 = \frac{1}{1 + K_{H,1}[H^+]_{loc} + K_{H,1}K_{H,2}[H^+]_{loc}{}^2} \quad (8)$$

$$f_2 = \frac{K_{H,1}[H^+]_{loc}}{1 + K_{H,1}[H^+]_{loc} + K_{H,1}K_{H,2}[H^+]_{loc}{}^2} \quad (9)$$

$$f_3 = \frac{K_{H,1}K_{H,2}[H^+]_{loc}{}^2}{1 + K_{H,1}[H^+]_{loc} + K_{H,1}K_{H,2}[H^+]_{loc}{}^2} \quad (10)$$

f_1, f_2, and f_3 correspond to fractional coverages of the $\equiv TiO^{-4/3}$, $\equiv TiOH^{-1/3}$, and $\equiv TiOH_2{}^{+2/3}$ surface groups, respectively. Sum of f_l is always 1. Surface charge density in such a formulation is given by

$$\sigma_j = e\Gamma\sum_{l=1}^{3} z_l f_l \quad (11)$$

where index j = i or o defines the inner or outer surface and z_1 is the charge of the surface group l. σ_i and σ_o are functions of electrostatic potentials at the two solid/electrolyte solution interfaces.

2.2. Electrostatics of the System. To study the surface charge properties of the TiO_2 NT, the classical density functional theory of nonuniform fluids coupled with a simple charge regulation method (explained above) is used. If the ions are considered as point-like charges with no correlations and only the electrostatic interaction is taken into account, then the grand canonical potential can be written as[39]

$$\Omega[\rho_\alpha(r)] = k_BT\sum_\alpha \int d^3r\rho_\alpha(r)\left(\ln\left(\frac{\rho_\alpha(r)}{\rho_\alpha^0}\right) - 1\right) + k_BT\int\sum_\alpha z_\alpha\rho_\alpha(r)\Phi(r)\, d^3r \quad (12)$$

where $\rho_\alpha(r)$ and z_α are one-body ion densities and the charge of the ions α, respectively. ρ_α^0 is the reservoir ion concentration, while $\Phi(r) = e\Psi(r)/k_BT$ is the "dimensionless" potential calculated from the Coulomb law. $\Psi(r)$ is the electrostatic potential, e is the elementary charge, k_B is the Boltzmann constant, and T is the thermodynamic temperature. Minimization of the grand canonical functional yields usual Boltzmann distributions

$$\rho_\alpha(r) = \rho_\alpha^0 \exp(-z_\alpha\Phi(r)) \quad (13)$$

The system satisfies the Poisson equation. Note that experiments made for this study are with 1 mM concentration of $NaNO_3$; therefore, the validity of this approach is assured. Inserting eq 13 into this electrostatic relation leads to the Poisson–Boltzmann equation which can be solved for any mixture of the electrolyte. In the cylindrical coordinate system with respect to symmetry, the Poisson–Boltzmann equation reads

$$\frac{d^2\Phi(r)}{dr^2} + \frac{1}{r}\frac{d\Phi(r)}{dr} = -4\pi l_B\sum_\alpha z_\alpha\rho_\alpha^0 \exp(-z_\alpha\Phi(r)) \quad (14)$$

where $\frac{d^2}{dr^2} + \frac{1}{r}\frac{d}{dr}$ is the radial component of the Laplace operator, $l_B = e^2/4\pi k_BT\epsilon_0\epsilon_{r,1}$ is the Bjerrum length, and ϵ_0 is the vacuum permittivity. $\kappa = (4\pi l_B\sum_\alpha z_\alpha{}^2\rho_\alpha^0)^{1/2}$ is the inverse Debye length.

Because both inner and outer cylinder surfaces are in contact with an electrolyte solution, the problem of finding an electrostatic profile consists of solving two coupled nonlinear second-order differential equations with two sets of boundary conditions. The boundary conditions are given by Gauss's Law.[40] Because of the symmetry, in the center of the cylinder,

DOI: 10.1021/acsami.7b18737
ACS Appl. Mater. Interfaces XXXX, XXX, XXX−XXX

the electric field becomes zero. The first boundary condition for the dimensionless potential is therefore

$$\left.\frac{\mathrm{d}\Phi(r)}{\mathrm{d}r}\right|_{r=0} = 0 \tag{15}$$

Note that even though the electric field along the cylinder axis is zero, the ions can still diffuse inside TiO_2 NTs because of the gradient of concentrations. Even if we consider the length of TiO_2 NTs on the micrometer scale, the system is fully equilibrated within few milliseconds. If the Gauss surface encloses volume very close to the inner cylinder surface ($r \rightarrow R_i$), then the second boundary condition states

$$\left.\frac{\mathrm{d}\Phi(r)}{\mathrm{d}r}\right|_{R_i} = \frac{e\int_0^{R_i}\rho_{el,1} r\ \mathrm{d}r}{\varepsilon_0\varepsilon_{r,1}k_BTR_i} \tag{16}$$

where $\rho_{el,1}$ is the electrolyte charge density inside of cylinder. The electrolyte charge density is defined by

$$\rho_{el,j}(r) = e\sum_{\alpha=1}^{N} z_\alpha\rho_\alpha(r) \tag{17}$$

where index j defines inner or outer cylinder cases. Throughout the article, the charge per unit length will be discussed, as was earlier mentioned by stating that edge effects are neglected.

The dimensionless electrostatic potential through the TiO_2 layer is obtained by applying the Gauss Law

$$\frac{\mathrm{d}\Phi(r)}{\mathrm{d}r} = -\frac{e\int_0^{R_i}\rho_{el,1} r\ \mathrm{d}r}{\varepsilon_0\varepsilon_{r,2}k_BTr} - \frac{e\sigma_iR_i}{\varepsilon_0\varepsilon_{r,2}k_BTr} \tag{18}$$

The integration of eq 18 gives

$$\Phi(r) = \Phi(R_i) + \frac{e\int_0^{R_i}\rho_{el,1} r\ \mathrm{d}r}{\varepsilon_0\varepsilon_{r,2}k_BT}\ln\left(\frac{R_i}{r}\right) + \frac{e\sigma_iR_i}{\varepsilon_0\varepsilon_{r,2}k_BT}\ln\left(\frac{R_i}{r}\right) \tag{19}$$

for $R_i \le r \le R_o$. The integration constant $\Phi(R_i)$ was determined from continuity of the potential at the inner TiO_2 NT surface.

Up to this point, the dimensionless potential inside the cylinder and through its walls is obtained. Next thing is to set boundary conditions for the outer surface which is in contact with the outer electrolyte solution (characterized by $\epsilon_{r,2}$). At the outer cylinder surface ($r \rightarrow R_o$), the Gauss theorem expresses the electric field as a function of the total internal charge. The latter is a sum of the volume integral of the inner cylinder electrolyte charge density and charge on the inner and outer surfaces. Consequently, the boundary condition for the potential outside the cylinder reads

$$\left.\frac{\mathrm{d}\Phi(r)}{\mathrm{d}r}\right|_{R_o} = -\frac{e\int_0^{R_i}\rho_{el,1} r\ \mathrm{d}r}{\varepsilon_0\varepsilon_{r,1}k_BTR_o} - \frac{e\sigma_iR_i}{\varepsilon_0\varepsilon_{r,1}k_BTR_o} - \frac{e\sigma_o}{\varepsilon_0\varepsilon_{r,1}k_BT} \tag{20}$$

Far from the cylinder's outer surface, the potential becomes zero

$$\Phi(r \gg \kappa^{-1}) = 0 \tag{21}$$

The solution of eq 14 for both cases (inside and outside) with respect to boundary conditions yields the dimensionless potential which is at the end converted to the electrostatic potential $\Psi(r) = k_BT\Phi(r)/e$.

The algorithm for finding a solution of two coupled second-order nonlinear second-order differential equations (eq 14) is based on a self-consistent approach. The calculations have been made on a pH scale to decrease the numerical noise which can be severe when dealing with proton concentrations. The rejection algorithm is the following:

1. Calculate $\sigma_i(\Phi_i)$ and $\sigma_o(\Phi_o)$ for the inner surface potential $\Phi_i(R_i) = 0$ and outer surface potential $\Phi_o(R_o) = 0$ (for the first three points only).
2. Find $\Phi_i(R_i)$ and $\Phi_o(R_o)$ with previously calculated $\sigma_i(\Phi_i)$ and $\sigma_o(\Phi_o)$.
3. Calculate again $\sigma_i(\Phi_i)$ and $\sigma_o(\Phi_o)$ but now with newly acquired values of surface potentials $\Phi_i(R_i)$ and $\Phi_o(R_o)$.
4. Repeat the procedure until two consecutive calculations do not provide different σ_i and σ_o (up to the convergence limit).
5. When the convergence is achieved, calculate again the electrostatic potential.

To guarantee and accelerate the convergence of the calculated surface charge densities, Aitken's δ^2 numerical accelerator was used.[41] The initial guess for surface charge densities at given pH was the extrapolated value from the second-order Lagrange polynomial.

2.3. Autoprotolysis of Water. The autoprotolysis of water (eq 6) occurs everywhere in space. In the present algorithm, it is assumed only in the reservoir. Nevertheless, considering the mathematical form of the equation, it is in fact valid anywhere in space, as can be understood from the following argument.

When the potential Ψ is not zero, the generalization of the mass action law is

$$\begin{aligned}\mu_w &= \mu_{H^+} + \mu_{OH^-}\\ &= \mu^\circ_{H^+} + k_BT\ln\frac{\rho_{H^+}}{\rho^\circ} + e\Psi + \mu^\circ_{OH^-} + k_BT\ln\frac{\rho_{OH^-}}{\rho^\circ} - e\Psi\end{aligned} \tag{22}$$

where μ_w, μ_{H^+}, and μ_{OH^-} are the chemical potentials of water, H^+, and OH^-, respectively. $\mu^\circ_{H^+}$ and $\mu^\circ_{OH^-}$ are standard chemical potentials of H^+ and OH^-, while ρ° is the concentration of the standard state. Consequently, because H^+ and OH^- have an opposite charge, the mass action law (eq 6) is not modified. The autoprotolysis of water is valid if the equality

$$\rho_{H^+}\rho_{OH^-} = K_w \tag{23}$$

is true anywhere. The latter equality is automatically satisfied by the Poisson–Boltzmann equation because

$$\rho_{H^+}(r) = [H^+]_0\exp(-e\Psi(r)/k_BT) \tag{24}$$

while the local hydroxide concentrations are equal to

$$\rho_{OH^-}(r) = [OH^-]_0\exp(e\Psi(r)/k_BT) \tag{25}$$

so that we recover the same equilibria as the one in the reservoir.

3. EXPERIMENTAL SECTION

3.1. Materials. For the synthesis of the TiO_2 NTs, the TiO_2 P25 (75% anatase, 25% rutile) from Degussa was used. The NaOH solution used (c = 10 mol dm^{-3}) was prepared by dissolving the NaOH pellets (Riedel-de-Haën) in the CO_2-free deionized water (the CO_2 was removed by boiling and bubbling of the deionized water with

DOI: 10.1021/acsami.7b18737
ACS Appl. Mater. Interfaces XXXX, XXX, XXX−XXX

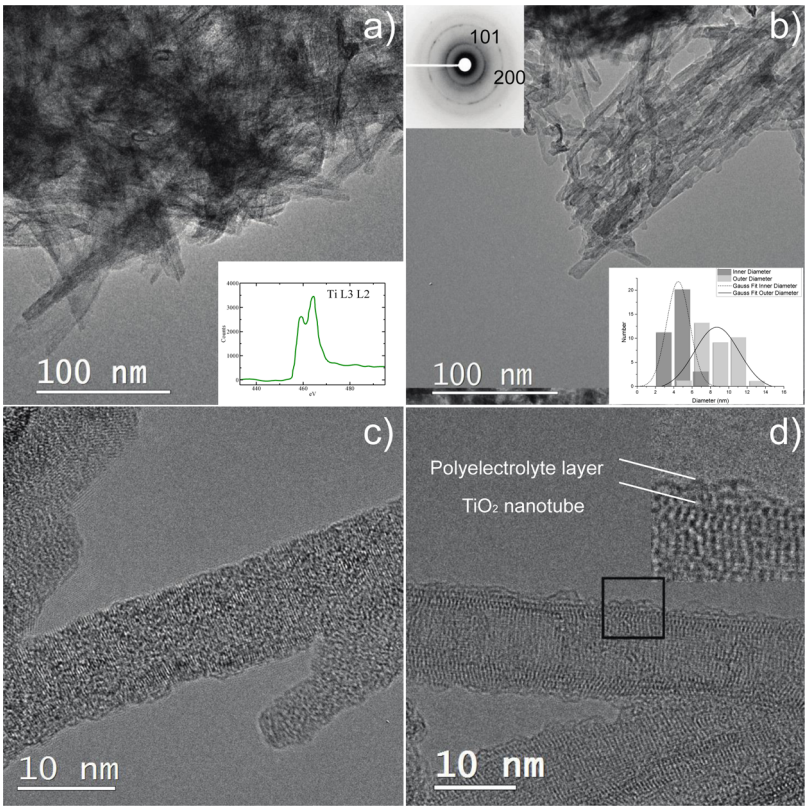

Figure 2. HR-TEM micrographs of TiO_2 NTs. (a) Few hundred nanometer-sized TiO_2 NTs with a characteristic EELS spectrum of poorly crystalized titania (inset), (b) TEM image of functionalized NTs with the selected area electron diffraction pattern in the upper left and distribution curve in terms of the inner and outer radii of TiO_2 NTs in the lower right corner inset. Two visible circles were indexed as 101 and 200 anatase planes, (c) pure TiO_2 NT with a clean and flat surface, and (d) functionalized TiO_2 NT surface with the polyelectrolyte where rough 1−2 nm sized layers could be observed at the surface (inset).

N_2). $NaNO_3$ was analytical grade and was purchased from Fluka. HNO_3 (c = 0.1 mol dm^{-3}) and NaOH (c = 0.1 mol dm^{-3}) titrival were obtained from Riedel-de-Haën. Tris(hydroxymethyl)aminomethane was obtained from Sigma-Aldrich. Five standard buffers, pH = 2, 4, 6, 8, and 10 that were purchased from Riedel-de-Haën were used for the potentiometric measurements, that is electrode calibration. Polydiallyldimethylammonium chloride (PDDA, molar mass 100−200 kDa; 20% wt, density 1.04 g cm^{-3}) which was used as a titrant was purchased from Sigma-Aldrich.

3.2. Synthesis of the TiO_2 NTs. TiO_2 NTs were prepared by the alkaline hydrothermal routine by suspending 2.0 g of TiO_2 P25 (75% anatase, 25% rutile) in aqueous 65 cm^{-3} NaOH solution (c = 10 mol dm^{-3}).[7] The suspension was stirred with a magnetic stirrer, and the ultrasound (1500 V, 20 kHz, Sonicator Ultrasonic Processor XL, Misonix Inc.) was applied to achieve homogeneity, using the following procedure: 5 min on followed for by 5 min off. The procedure lasted for a total of 2 h. The prepared homogeneous suspension was placed in the Teflon lined autoclave. Synthesis temperature was maintained at Θ = 146 °C for 48 h. The obtained sample was filtered and washed with deionized water until the conductivity has approached to approximate conductivity of deionized water (κ < 10 μS cm^{-1}). The sample was incubated with 0.1 M HCl for 3 h to remove excess of the adsorbed sodium ions. The resulting sample was again filtered and washed with deionized water until the conductivity of the supernatant was below 10 μS cm^{-1}. The TiO_2 NTs were dried at 80 °C for 6 h in the air and stored in a glass bottle.

3.3. Characterization of the TiO_2 NTs. The morphology and size of TiO_2 NTs were studied by HR-TEM. A 200 kV Cs probe-corrected cold-field-emission transmission electron microscope (Jeol ARM 200 CF), coupled with a Gatan Quantum ER electron energy-loss spectroscopy (EELS) system and an energy-dispersive X-ray spectroscopy (EDXS) system Jeol Centurio with a 100 mm^2 SDD detector, was used. Samples with TiO_2 NTs powder were dispersed in ethanol and placed on a copper lacy-carbon grid. EELS and EDXS spectra and mappings were collected in a scanning transmission mode.

3.4. Electrophoretic Mobility of the TiO_2 NTs. Electrophoretic mobility of the TiO_2 NTs was determined using the Zetasizer Nano ZS (Malvern, UK) equipped with a green laser (λ = 532 nm). The intensity of the scattered light was detected at the angle of 173°. For electrokinetic measurements, the TiO_2 NT suspension with a mass concentration, γ = 0.1 g dm^{-3}, was prepared in the 0.001 mol dm^{-3} $NaNO_3$ aqueous solution. Initial pH was adjusted with NaOH (c = 0.1 mol dm^{-3}). Suspensions were sonicated for 3 min using the bath sonicator (35 kHz, 320 W, Bandelin Sonorex Rk 100 H) before mobility measurements.[42] The electrophoretic mobility of the TiO_2 NTs as a function of pH was measured where HNO_3 (c = 0.1 mol dm^{-3}) was used as a titrant. After each addition of HNO_3, the system was left for equilibration for 10 min to obtain a stable pH electrode signal response with the potentiometer accuracy of 0.01 mV. To prevent sedimentation, stirring was applied during the measurement. Then, pH was recorded with a combined microglass electrode (6.0228.010, Metrohm) which was calibrated with five standard buffers (pH = 2, 4, 6, 8, and 10). All experiments were carried under a nitrogen atmosphere at Θ = (25 ± 0.1) °C. Data were collected with five runs per measurement for two measurements in total. All data processing was done by the Zetasizer software 6.32 (Malvern instruments).

3.5. Surface Charge Density of the TiO_2 NTs. Surface charge density analysis of the NTs was measured with Mütec-PCD05 (BTG Instruments, Switzerland). TiO_2 NT (1 g dm^{-3}) suspension was prepared by suspending 25 mg of solid NTs in 25 mL of aqueous $NaNO_3$ [$c(NaNO_3)$ = 0.001 mol dm^{-3}] solution. To increase homogeneity, the suspension was shaken and then the sonication treatment was applied twice for 3 min. Suspensions for PCD titrations

DOI: 10.1021/acsami.7b18737
ACS Appl. Mater. Interfaces XXXX, XXX, XXX−XXX

(as well as for the electrophoretic measurements mentioned before) were sonicated with medium power and sonication treatment lasting only 3 min, to prevent the breakage of the TiO_2 NTs. The procedure was repeated twice for each suspension. The mechanical breakage of TiO_2 NTs has been reported before.[10,43] The pH of suspension was adjusted with NaOH (c = 0.1 mol dm^{-3}). The suspensions with pH between 2 and 10 were prepared. The suspension was added into the Mütec-PCD05 cell. The polyelectrolyte titrant solution, c(PDDA) = 1.3 × 10^{-4} mol dm^{-3}), was added in the Mutek-PCD05 sample cell containing the suspension of TiO_2 NTs. The streaming potential signal was monitored as titration is conducted. The PDDA denotes the concentration of the monomer (diallyldimethylammonium chloride) units. The titration was conducted manually. After the streaming potential signal changed sign, the procedure was stooped, and total charge σ_{tot} (C g^{-1}) of particles was computed from:

$$\sigma_{tot} = \frac{Fc(\mathrm{PDDA})V(\mathrm{PDDA})}{m(\mathrm{TiO_2})s} \quad (26)$$

where s is the specific surface area in m^2 g^{-1}, F is Faraday's constant in C mol^{-1}, c(PDDA) is the concentration of the titrant, V(PDDA) is the volume of the titrant necessary to obtain the point of the zero charge, and $m(TiO_2)$ is the mass of the TiO_2 NTs added in the suspension. Specific surface s of TiO_2 NTs sample is obtained from Brunauer–Emmett–Teller measurements and is 200 m^2 g^{-1}. The total charge per unit of mass was converted to charge per unit length $Q_{tot}L^{-1}$ in C m^{-1}.

4. RESULTS AND DISCUSSION

4.1. Experimental Results and the Fitting Procedure.

The TiO_2 NTs were few hundreds nanometer long and around 12 nm thick (Figure 2a).

From TEM images, it was concluded that they were mainly double-walled and showed a faint and diffuse electron diffraction pattern, indicating very poor crystallinity. After the synthesis, the analyzed TiO_2 NTs were not annealed at high temperature, so there is a lot of amorphous mass present within the TiO_2 NTs sample. Two visible circles in the diffraction pattern could be indexed as (101) and (200) planes of anatase (inset Figure 2b), still, other lines are missing which is characteristic of incomplete crystallinity. The same could be concluded from the EELS spectrum (inset Figure 2a), where Ti L3 and L2 edges were observed without crystal splitting, characteristic for fully crystalline material with the +4 valence state of titanium (like in anatase, rutile, or brookite). Evidence that we successfully functionalized the TiO_2 NT surface with the polyelectrolyte is seen in Figure 2d where 1–2 nm thick layer of organic material with different contrasts could be observed (inset shows the surface at higher magnification). The sample of the polyelectrolyte-functionalized TiO_2 NT corresponds to residue after charge determination in Mutek-PCD05. The nonfunctionalized TiO_2 NT has a clean and smooth surface, as shown in Figure 2c.

Figure 3 represents the electrophoretic mobility of the TiO_2 NTs in 0.001 M $NaNO_3$ aqueous electrolyte solution.

The results of electrophoretic mobility measurements are given for a qualitative purpose only. The reason is in the fact that we have investigated hollow cylindrical particles of various sizes for which the evaluation of ζ-potential through the Smoluchowski equation is not valid. Therefore, no quantitative conclusion about the surface charge properties can be drawn. Yet, few things can be noted. First, the shape of the mobility μ as a function of the pH curve reveals the asymmetry with respect to the isoelectric point, pH_{iep}, which is a consequence of the asymmetric charges of anatase phase surface groups. The isoelectric point pH_{iep} is around pH = 3.6. In the pH region above pH_{iep}, the outer surface of the TiO_2 NTs is negatively

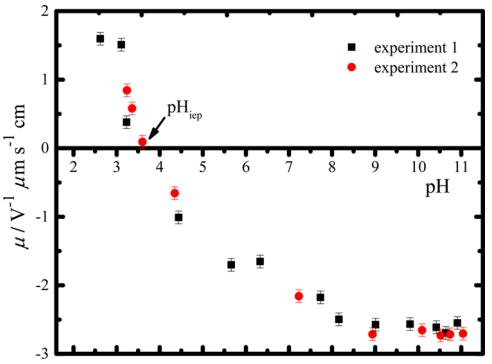

Figure 3. Electrophoretic mobility of the TiO_2 NTs in $NaNO_3$ aqueous electrolyte solution as a function of pH. γ = 0.1 g dm^{-3}, $c(NaNO_3)$ = 0.001 M, T = 298 K. The results of the two measurements are presented.

charged, whereas in that below pH_{iep} the surface is positively charged. One more thing to add here is the plateau which is achieved at pH values higher than 9. Such a regime is a consequence of high surface charge of TiO_2 NTs, which is typical for fully deprotonated surface sites.

The results of the polyelectrolyte titration are presented in Figure 4 along with the predictions of the model. The

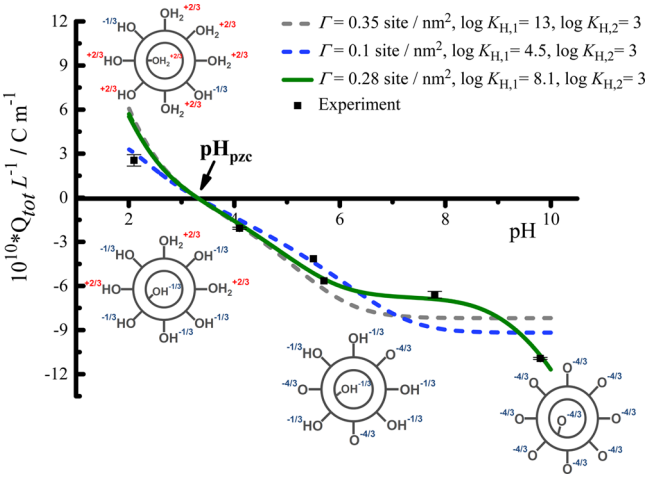

Figure 4. Determination of TiO_2 NT total charge by the polyelectrolyte titration. The data are expressed in charge per unit of length as a function of pH. Black squares denote experimental data whereas solid and dashed curves present possible fits. Schemes representing the charging process are added for the intuitive purpose. Both experimental data and model calculations are made at T = 298 K with $c(NaNO_3)$ = 0.001 M.

experimental data of total charge per unit of mass are converted to charge per unit of length. In this way, we avoid dealing with polydispersity in terms of length of TiO_2 NTs, which is substantial for this type of the materials. Similar considerations have already been reported.[44] The multiplication of charge per length (y-axis) and the average length of TiO_2 NTs provides the total average charge. The charge per unit of length can also be converted to surface charge density (with polydispersity taken into account). The order of magnitude for measured charge is only around 30 mC m^{-2} at pH = 10, that is, TiO_2 NTs are weakly charged.

The experimental data obtained by polyelectrolyte titration, as well as ζ-potential and potentiometric acid–base and mass

DOI: 10.1021/acsami.7b18737
ACS Appl. Mater. Interfaces XXXX, XXX, XXX–XXX

titration measurements provide an average total charge of examined samples. In the case of porous materials (including TiO_2 NTs), besides the total charge, no other conclusion can be accurately drawn about the fractions of charge in the pores. It follows that the results of these methods can be safely interpreted for charge determination of nonporous materials only, that is, the ones that have a simple shape and well-defined surface planes (for a single crystal). For all other cases, a theoretical description of charging is needed.

In the case of TiO_2 NTs, the total compensated charge during the polyelectrolyte titration is, in fact, the sum of three terms: the charge of the electrolyte solution confided inside of the TiO_2 NT, the charge at the inner surface, and the charge at the outer surface of the TiO_2 NT

$$Q_{tot} = 2\pi L \int_0^{R_i} \rho_{el,1} r \, dr + \sigma_i 2\pi L R_i + \sigma_o 2\pi L R_o \quad (27)$$

with L being the average length of TiO_2 NTs and σ_i and σ_o being the inner and outer surface charge densities. The first term is the volume integral of electrolyte charge density inside of TiO_2 NTs. The second and the third terms are a charge on the inner and outer TiO_2 NT surfaces and are obtained by multiplying surface charge densities with appropriate surface areas. The first term is always of the opposite sign compared to the surface charge densities and it lowers total charge that is compensated during the titration. If we divide both sides by L, the total compensated charge per unit of length is obtained

$$Q_{tot} L^{-1} = 2\pi \int_0^{R_i} \rho_{el,1} r \, dr + \sigma_i 2\pi R_i + \sigma_o 2\pi R_o \quad (28)$$

A charge per unit length is plotted in Figure 4 as a function of pH. It is crucial to emphasize that interpretation of data we report here is specific to the experimental setup, as should be always done when dealing with complex porous systems. During the titration inside of the Mütec-PCD05 titration cell, the polyelectrolyte binds to the outer surface of TiO_2 NTs under the influence of moving piston, creating the pressure and strong electrostatic forces between these colloids.[45,46] The polyelectrolyte is under the influence of the electric field created by the total charge Q_{tot} enveloped by the Gaussian surface (eqs 27 and 28).

In measurements, we used a high molar mass polyelectrolyte at 1 mM $NaNO_3$ solution. In this way, we made sure that the polyelectrolyte cannot penetrate inside the TiO_2 NTs, thus violating eq 27. Moreover, at 1 mM salt concentrations (which are the physical conditions of our system), the polyelectrolyte has fully stretched conformation, so it is safe to assume the accuracy of the method. It is worth to mention that HR-TEM measurements of the titrated sample show that the polyelectrolyte binds to the TiO_2 NT outer surface in the monolayer. This finding is important to justify the assumed 1:1 stoichiometry in titration. The results can be found in Figure 2d.

The results presented here (the point of zero charge and low charge per length values) are in accordance with those obtained by previous studies of the TiO_2 NT system.[10] Interestingly, in both present and past studies, the charge of TiO_2 NTs is typically one order of magnitude smaller than the charge of distinct morphologies, namely, TiO_2 nanowires or nanosheets.

Fitting the experimental data with the model can provide different explanations of the system, but only few physically make sense. We have identified and described three distinct cases and presented them in Figure 4. The calculated point of zero charge, pH_{pzc}, is in our model determined by the second intrinsic protonation constant log $K_{H,2}$ = 3. According to the experiment, we fixed the value of it for all three possible fits. This means that we needed to simultaneously fit the two parameters, namely, the surface site density Γ and the first intrinsic protonation constant log $K_{H,1}$. In the literature, various cases of fitting were reported (note that up to our knowledge, none for TiO_2 NTs). The reported differences between log $K_{H,1}$ and log $K_{H,2}$ ranged from 1 up to 20.[47,48] To make a clear distinction on how experimental data can be interpreted, we have decided to describe all three distinct cases separately. The first case is when log $K_{H,1}$ and log $K_{H,2}$ are close, and it corresponds to the blue dashed curve in Figure 4. If one assumes such parameters, then the interpretation of data would be that already at pH = 7, there is a saturation of surface charges because all surface groups are in fact fully deprotonated $\equiv TiO^{-4/3}$ groups. f_1 dominates the sum in eq 11. The charge of TiO_2 NTs is constant throughout all higher pH values. Although interesting, this way of fitting cannot properly account for the measured values of charge at high pH. The opposite case is presented as a gray dashed curve. Now the log $K_{H,1}$ equals 13. Even if the log $K_{H,1}$ is much higher, results are globally the same. If this set of parameters is used, then there is again the plateau after pH = 6.5, but now it does not represent the population of $\equiv TiO^{-4/3}$ but $\equiv TiOH^{-1/3}$ surface groups. Now f_2 dominates in the sum in eq 11. Because log $K_{H,1}$ is high, an extremely high pH (unreachable by an experiment) is needed to deprotonate $\equiv TiOH^{-1/3}$ surface groups. As in the previous case, it can be seen that the gray dashed curve cannot properly describe experimental data at high pH.

The third case is the green solid curve in Figure 4 which corresponds to log $K_{H,1}$ = 8.1. As can be seen, the green curve predicts a steep increase of the TiO_2 NTs charge with increasing pH. When pH is little less, but still near 8, the population of $\equiv TiO^{-4/3}$ increases and so the overall charge of TiO_2 NTs increases. The small plateau in the region between pH = 6 and 8 corresponds to the region where $\equiv TiOH^{-1/3}$ surface groups dominate in the expression for surface charge density (eq 11).

Because the green curve provided the best fit of the experimental data, we considered that Γ = 0.28 site/nm^2 and log $K_{H,1}$ = 8.1 are the most accurate (i.e., realistic) set of parameters that uniquely describes the experimental data. This choice of log $K_{H,1}$ has been justified from a small theoretical argument. As presented in the Appendix, if the association of ions at the site is driven mainly by electrostatic force, for example, as in the Born model or the MUSIC approach,[48] we can estimate the difference log $K_{H,2}$ − log $K_{H,1}$. Indeed, within the framework of the McMillan−Mayer theory, the protonation constants can be written as a typical Bjerrum association[29,49,50]

$$K^{\circ}_{H,1} = \int_{V_{site,1}} e^{-\beta U(\mathbf{r})} d^3 r \quad (29)$$

where $K^{\circ}_{H,1}$ represents protonation constants, $V_{site,l}$ volume of sites accessible to protons, index l denotes a type of surface group, and $U(\mathbf{r})$ is solvent-averaged potential between the oxygen atom and the proton. In this calculation, $U(\mathbf{r})$ is assumed to be purely Coulombic. For log $K_{H,1}$ = 8.1 and log $K_{H,2}$ = 3, we obtain the distance between an oxygen atom and a proton to be equal 0.64 Å. That is the reasonable bond length, and it does justify the use of log $K_{H,1}$ = 8.1 and log $K_{H,2}$ = 3 for further calculations and exploration of charge properties of TiO_2 NTs. The same calculations for other sets of intrinsic

DOI: 10.1021/acsami.7b18737
ACS Appl. Mater. Interfaces XXXX, XXX, XXX−XXX

protonation constants yield unrealistic results. The entire derivation and calculated bond lengths for other sets of constants are given in Appendix.

Another thing to address is a rather low surface site density Γ obtained through a fitting procedure. In every possible fit, the value of Γ was always below 1 site/nm^2. In the case of anatase phase colloid particles, a majority of previous work report surface site densities larger than 1 site/nm^2.[34] It must be noted that these studies were made for the flat interface. In our study, we examine a highly curved interface on the nanometer scale. Still, even the low site density we obtained through the fitting procedure results in values of normalized surface charge densities that are usually used in classical density function theory, molecular dynamics calculations, and so forth.[51−53]

In fact, to predict experimental data, one may take a few possible routes. One route is to fix the point of zero charge according to the experimental data and to assume a priori high surface site density and then to fit the intrinsic protonation constants for one or more surface groups. This approach has proven useful in predicting ζ-potential of colloids. Still, we argue that it is not a proper way of fitting because Γ, log $K_{H,1}$, and log $K_{H,2}$ are dependent.[36] Sometimes, to achieve the steep increase of charge, the additional type of surface groups is introduced. This way imposes additional two parameters, namely, new intrinsic protonation constants and the site density of the new surface group. The third approach consists of allowing the association of the supporting electrolyte with charged surface groups as usual competition reactions. The higher association constant of metal cations (compared to anions) causes decrease of the total charge, and thus higher surface site densities Γ can be obtained in the fitting process. Note that this approach also adds two additional adjusted parameters.

The results obtained by this study arose from the intent of authors to make a model with the lowest possible number of parameters. A shape of the titration curve, values of total charge, and the point of zero charge are the consequence of solution of two coupled nonlinear Poisson−Boltzmann equations along with charge-regulated boundary conditions with log $K_{H,2}$ = 3 fixed accordingly to experimental data and two adjustable parameters Γ = 0.28 site/nm^2 and log $K_{H,1}$ = 8.1. It is assumed that one type of surface sites can undergo two consecutive protonations depending on the pH.

It must be noted that from the practical point of view, the preparation of samples for charge determinations in the case of TiO_2 NTs is a difficult task. Besides by our group, the mechanical damage of TiO_2 NTs upon the ultrasonic treatment was previously reported by other authors.[10,43] The breakage of TiO_2 NTs was reflected on their properties in an aqueous solution, that is, ion-exchange kinetics. To overcome that difficulty, the ultrasound was applied during short intervals (the procedure can be found in the Experimental Section). Within such a procedure, it is intuitive that a large portion of TiO_2 NTs remains attached into a larger agglomerate. Agglomeration caused a decrease of the specific surface exposed to aqueous solution, which results in lower total charge measured. In this manner, the Γ values obtained through fitting procedure are lower. These results are consistent with finding known from the literature.[43] Also, it was noted at the beginning of this section that the sample analyzed by HR-TEM has shown a high degree of an amorphous phase. With such an experimental evidence, we understand that the value of Γ cannot be predetermined, and it has to be somewhat adjusted. Moreover, the choice we made (not to fix Γ) has another advantage. If the intrinsic protonation constants are known and their values can be assumed to be reliable, then the model can predict surface site densities for porous materials. A vice versa deduction also applies. A predictive method is crucial for the study of any ion behavior in confined media.

The main objective of this work was to exploit the utility of the set of nonlinear Poisson−Boltzmann equations to understand the charge properties of TiO_2 NTs. Therefore, in the following subsection, we present the results of the calculations for the system of an infinitely long cylinder immersed in the aqueous solution for various physical conditions (pH, reservoir salt concentrations). All subsequent calculations were made with values of parameters Γ = 0.28 site/nm^2, log $K_{H,1}$ = 8.1, and log $K_{H,2}$ = 3 at T = 298 K. Once again, we must emphasize that using other two sets of parameters would greatly influence the interpretation of charge properties. The calculations were done, but they are not incorporated into this article.

4.2. Electrostatic Properties of TiO_2 NTs. The solution of the system of coupled nonlinear Poisson−Boltzmann equations (eq 14) is presented in Figure 5. The electrostatic potentials

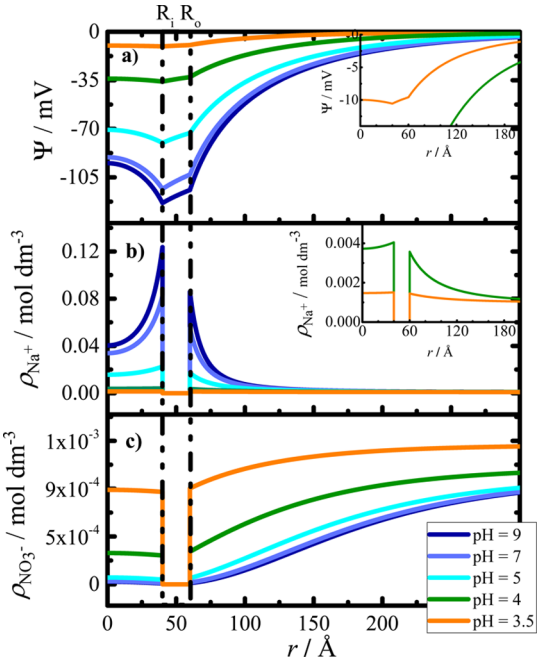

Figure 5. Results of the calculation: (a) electrostatic potential profiles; (b) equilibrium counterion profiles; (c) equilibrium coion profiles; T = 298 K, c_0 = 0.001 M, Γ = 0.28 site/nm^2, log $K_{H,1}$ = 8.1, log $K_{H,2}$ = 3.

and counter and coion profiles are plotted for five different pH values. The supporting electrolyte concentration is 0.001 M. In the experiment, we used $NaNO_3$, but within the model, no ion specificity is taken into the account. Debye length κ^{-1}, for such conditions, is around 96 Å.

Figure 5a shows the electrostatic potentials from the center of the cylinder up to some point away from the outer surface. The calculations have shown that there is a nonzero electrostatic potential along the cylinder axis but the electric field is equal to 0. Therefore, the boundary conditions are satisfied. The region from 40 to 60 Å represents the electrostatic potential through the TiO_2 layer and is described by a monotonic increasing function (eq 19). The difference in surface electrostatic potentials at the inner and outer surfaces

DOI: 10.1021/acsami.7b18737
ACS Appl. Mater. Interfaces XXXX, XXX, XXX−XXX

causes asymmetry in ion distributions (as shown in Figure 5b). The Figure 5c shows the equilibrium concentrations of coions inside the cylinder.

At high pH, the negatively charged TiO_2 NTs exhibit an electric field which attracts counterions (Na^+) near the surface and repels coions (NO_3^-). Because the Debye length is more than twice the inner radius of TiO_2 NTs, it is understandable that at high pH calculated coion concentrations are negligible. At lower pH values, closer to the point of zero charge, the counterion concentrations near the surface are still higher compared to the bulk, but now the coion concentrations are greatly increased. Such results are expected because with lowering of surface charge, the screening becomes inefficient. The screening of the inner surface charge as a function of pH is given in Figure S2 in the Supporting Information. The calculation has shown that around the point of zero charge, around only 30% of the inner surface charge is screened by the inner cylinder electrolyte solution. As a consequence, with decreasing pH, the asymmetry in ion distributions diminishes and can be clearly seen for pH values 4 and 3.5 (note that pH_{pzc} is roughly at pH = 3.3). The values of reservoir salt concentrations and values of the inner TiO_2 NT radius for which NO_3^- coions can more easily penetrate inside of TiO_2 NTs are studied separately later in this article.

To solve the Poisson–Boltzmann equation, the overall electroneutrality condition must be fulfilled.

$$2\pi L\int_0^{R_i} r\rho_{el,1}\,dr + 2\pi R_i L\sigma_i + 2\pi R_o L\sigma_o + 2\pi L\int_{R_o}^{\infty} r\rho_{el,2}\,dr = 0 \quad (30)$$

At the 0.001 M reservoir salt concentration, the electroneutrality is not fulfilled inside of the cylinder. Similar results have been obtained which are already reported.[54] The excess charge is then compensated at the outer surface by the electrolyte solution, and overall, the system is neutral. We made calculations with the higher value of the inner TiO_2 NT radius R_i. The thickness of the TiO_2 layer was kept constant at 2 nm and the reservoir salt concentration at 0.001 M. As the inner radius is increased, the asymmetry in terms of the electrostatic potential and ion distributions is lost, and the system starts to behave like a charged plate immersed in the electrolyte solution. Note that also the asymmetries in ion distributions are lost in the limit of zero-thickness of the TiO_2 layer.

Besides reproducing the experimental data, the model was used to give insights into charge properties at different conditions. The titration curves were calculated for different reservoir salt concentrations. The results are shown in Figure 6. The shape of the curves does not change considerably with the increase of the bulk salt concentrations. As is known from the literature, the increase in the reservoir salt concentration is followed by the increase in the charge of colloids.[55] Our calculations have shown the same trend. The origin of such increase in the charge is just a question of more efficient screening of the surface charge. For higher salt concentrations, the calculated surface potentials Ψ_i and Ψ_o are less negative (when discussing only the case where TiO_2 NTs are negatively charged). In this manner, the proton concentrations at the surface are decreased, therefore most of the surface groups remain deprotonated, i.e., more charge is detected. Practically, it means that within the titration experiment (polyelectrolyte titration or some other technique), the consumption of titrant increases when more salt is added into the system. From Figure 6, it can be seen that inflection points that describe the shape of the charging curve are at different positions (pH values) for different salt concentrations. The origin for such phenomena is the same as written previously. The change in calculated surface potentials governs the ratio of the population of charged surface groups and thus determines the value of charge at a particular pH value.

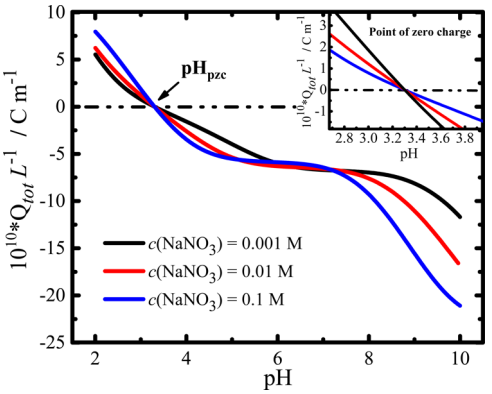

Figure 6. Calculated titration curves for three different reservoir salt concentrations: black line corresponds to $c(NaNO_3)$ = 0.001 M, red line corresponds to $c(NaNO_3)$ = 0.01 M, and blue line corresponds to $c(NaNO_3)$ = 0.1 M. The inset shows the enlarged pH region near the point of zero charge.

The inset in Figure 6 shows that all three curves have the same point of zero charge. In real systems, pH_{pzc} depends on reservoir salt concentrations and on the type of salt, as was found experimentally.[10] Our calculations showed no such difference. The explanation for such phenomena is rather simple. In the Theory section, we assumed the ideality of the solution. The (electro)chemical potential of ion H^+ is defined as follows: $\mu_{H^+} = \mu^{o}_{H^+} + k_B T \ln(\gamma_{H^+} c_{H^+}/c^{o}) + e\Psi$. At the point of zero charge, Ψ is equal to zero so the last term disappears. Because coefficients of activity are equal to 1, the intrinsic protonation constants are independent bulk salt concentrations, and thus the point of zero charge does not change.

The influence of dielectric constant $\epsilon_{r,2}$ through the TiO_2 layer has also been studied. Calculations were made with $\epsilon_{r,2}$ values 40, 80, and 120. The differences in total charge per unit length as a function of pH for those three values were very small in the region of high pH (Figure S1 in the Supporting Information). A better knowledge of the crystal structure of the TiO_2 NT layer would motivate further investigations about the influence of the dielectric constant on overall system charge properties.

Our calculations show that absolute value of surface charge density σ_o is larger than σ_i throughout the whole pH region (Figure 7). This finding is a consequence of the differences in the curvatures of the two surfaces ($R_o > R_i$). The surface charge density scales with the radius of TiO_2 NTs, and there are always more charges on the outer surface. Also, our calculations have shown that proton concentrations at the inner surface are higher when compared to the outer surface that is the higher proton adsorption/desorption at the inner surface. This means that there are less deprotonated surface groups, and therefore, less amount of charges. The two effects account for the differences in the amount of charge between the surfaces. A more informative way to distinguish the difference between the charge of the outer and the inner surface can be obtained if the

DOI: 10.1021/acsami.7b18737
ACS Appl. Mater. Interfaces XXXX, XXX, XXX–XXX

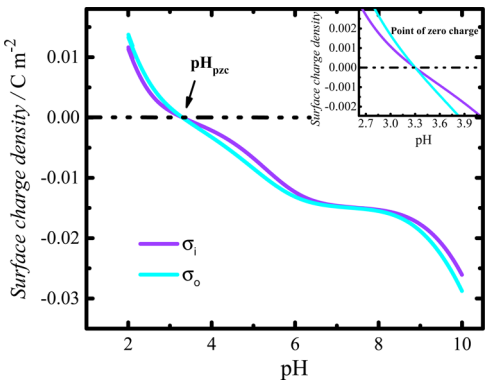

Figure 7. Calculated inner and outer TiO_2 NTs surface charge densities, σ_i and σ_o at $c(NaNO_3)$ = 0.001 M, T = 298 K, $\epsilon_{r,1}$ = 80. The average length of TiO_2 NTs assumed to be 100 nm (Figures 2b and S3).

ratio of the two is plotted as a function of pH. The charge at the surface is understood as the sum of charges from the surface groups only because we did not consider the association of the supporting electrolyte.

$$\frac{2\pi LR_o\sigma_o}{2\pi LR_i\sigma_i} = \frac{\sigma_o R_o}{\sigma_i R_i} \tag{31}$$

The ratio of the charge between the outer and the inner cylinder surface (eq 31) plotted as a function of pH in Figure 8

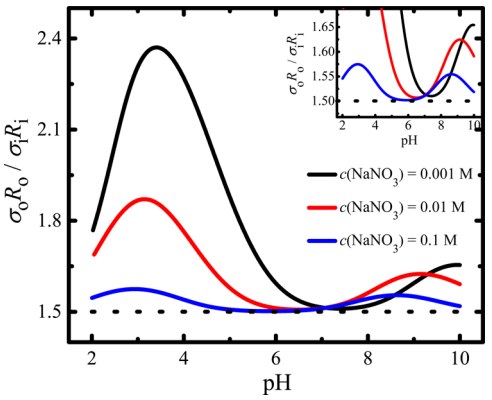

Figure 8. Fraction of the charge between the outer and the inner surface as a function of pH. The results are given for three different reservoir salt concentrations: black line corresponds to $c(NaNO_3)$ = 0.001 M, red line corresponds to $c(NaNO_3)$ = 0.01 M, and blue line corresponds to $c(NaNO_3)$ = 0.1 M.

shows that there is a pronounced increase of the charge at the outer TiO_2 NT surface near the point of zero charge, pH$_{pzc}$. A smaller increase can be seen also in the region above pH = 8. Besides the increase of the charge at the outer surface, there is also the leveling of the charge regime, as can be seen in the inset of Figure 8. It is in the region of pH between 6 and 8, depending on the reservoir salt concentrations. This leveling has a value 1.5 (roughly) and corresponds to the ratio of the inner and outer TiO_2 NT radius. It is the region where $\equiv TiOH^{-1/3}$ surface groups are most populated ones for both inner and outer surface (fractional coverage f_2 dominates the sum in eq 11).

First, we examine the curve calculated for the reservoir salt concentration equal to 0.001 M. The accumulation of charge at the outer surface when pH is close to values of intrinsic protonation constants can be understood from the following argument. Whenever the population of particular surface groups changes rapidly, which is the case when pH is near the value of the intrinsic protonation constant, even small differences between calculated Ψ_i and Ψ_o cause pronounced differences in surface charge densities. It is a reasonable consequence because surface charge density depends exponentially on the Ψ_i and Ψ_o (eq 24). Practically, this phenomenon means that the asymmetry in proton adsorption between the two surfaces is even more pronounced when pH is close to the value of intrinsic protonation constants. The largest difference is found for pH near pH$_{pzc}$ (or log $K_{H,2}$). The explanation of the phenomena is simple. At high pH, the surface groups are already mostly deprotonated and therefore less sensitive to the changes in surface potentials. This is reflected in small differences of charge between the inner and outer surfaces. When pH approaches pH$_{pzc}$, we are comparing almost no charge on the inner surface and more charge (more than twice) on the outer surface. This in turn generates such pronounced differences in charge. On more thing to notice in Figure 8 is the charge ratio curves for 0.01 and 0.1 M reservoir salt concentrations. The increase of reservoir salt concentrations causes the disappearance of differences between the amount of charge on the inner and the outer surface because of the more efficient screening (eq 19).

The Donnan effect in the case of the interior volume of TiO_2 NTs has also been analyzed. The results are presented in Figure 9. The ratio of the mean concentration of nitrate coions $\langle\rho_{NO_3^-}\rangle$

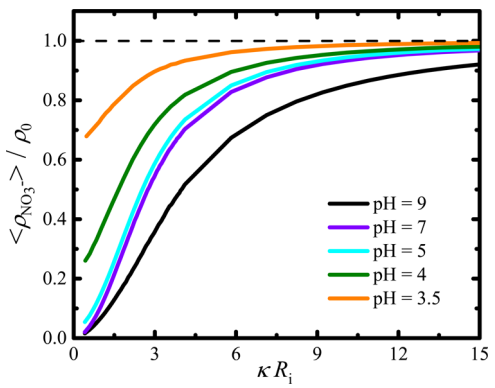

Figure 9. Study of the Donnan effect. $\langle\rho_{NO_3^-}\rangle/\rho_0$ is the ratio of the mean coion (NO_3^-) concentration inside TiO_2 NTs and the reservoir coion concentration. The results are shown for various reservoir pH values.

inside the cylinder to the reservoir salt concentration as a function of κR_i has been studied at different pH values. The mean concentration of NO_3^- is defined as

$$\langle\rho_{NO_3^-}\rangle = \frac{2\int_0^{R_i}\rho_{NO_3^-}(r)r\,dr}{R_i^2} \tag{32}$$

κR_i parameter varies either when the reservoir salt concentration is modified (the inverse Debye length κ is proportional to $\rho_0^{1/2}$) or when the inner radius R_i is greatly increased. At high pH, the electric field does not permit the penetration of NO_3^- ions. Moreover, the reservoir salt concentrations need to be very high to have a mean concentration equal to the reservoir salt concentration. It is the case when the surface charge is completely screened by counterions, namely, Na^+.

DOI: 10.1021/acsami.7b18737
ACS Appl. Mater. Interfaces XXXX, XXX, XXX−XXX

With a decrease of reservoir pH, surface charge density also decreases. When the electric field at TiO_2 NT inner surface is diminished (near the point of zero charge), NO_3^- ions can more easily penetrate inside. Just to emphasize how the strength of the electric field affects the ion distributions, let us once again study the two extreme cases of pH. For the pH = 9 in 0.001 M $NaNO_3$ system, there are almost no NO_3^- ions inside of the TiO_2 NTs at T = 298 K, whereas at pH = 3.5 for the same conditions, around 35% of the total amount of NO_3^- ions are already inside.

5. CONCLUSIONS

Within this study, we have presented a framework which clears the path to understand charge properties of TiO_2 NTs and other porous material in low salt aqueous solution.

With the HR-TEM, we have obtained the distributions of the inner and outer TiO_2 NTs radii. The electrophoretic mobility measurements at 0.001 M $NaNO_3$ showed that pH_{iep} of TiO_2 NTs is around 3.6. With the particle charge detector, we have measured the charge of TiO_2 NTs in 0.001 M $NaNO_3$. The measurements showed that TiO_2 NTs are weakly charged and pH_{pzc} is around 3.2.

The theoretical model was developed to understand and interpret the experimental data. The basis of the theoretical model includes the Poisson−Boltzmann equation (which is the simplest case of the classical density functional theory for electrolyte solutions) and the surface charge regulation method via the law of mass action. The solutions provided by the Poisson−Boltzmann approach are consistent with the molecular dynamics.[51,56] A system of two coupled nonlinear second-order differential equations was solved numerically in a self-consistent manner.

The experimental results were fitted with the theoretical model to obtain the surface site density Γ and intrinsic protonation constants log $K_{H,1}$ and log $K_{H,2}$. The three possible fits were addressed and discussed separately. As the best fit, we considered the one obtained for Γ = 0.28 site/nm^2, log $K_{H,1}$ = 8.1, and log $K_{H,2}$ = 3 (note that log $K_{H,2}$ was fixed by the surface charge density measurements and not simultaneously fitted). The plausibility of use of this set of parameters was justified with a theoretical calculation based on the Bjerrum-like contact ion pair formation model. Also, we emphasize that all adjusted parameters are sample-dependent and that greater care is needed for the interpretation of both calculated and experimental data.

The calculation of total TiO_2 NT charge with fitted values of Γ, log $K_{H,1}$, and log $K_{H,2}$ predicts a steep increase of the surface charge after pH = 8. At the 0.001 M concentration of $NaNO_3$, the inner TiO_2 NT surface charge is not fully compensated by the inner electrolyte solution, which causes the asymmetries in ion distributions. The overall electroneutrality of the TiO_2 NT system at low reservoir salt concentrations is achieved by the electrolyte solution outside of TiO_2 NTs. pH determines the surface charge density and therefore the screening of the interface by the ions in the solution. The screening of both TiO_2 NTs surfaces is more efficient at high reservoir pH. The total charge of TiO_2 NTs increases with the increase of the reservoir $NaNO_3$ concentration.

Furthermore, our calculations show that the ratio in charge between the inner and outer surfaces is also pH-dependent and is not always equal to the ratio of TiO_2 NT radii. The difference in charge between the two surfaces is diminished by an increase of the reservoir $NaNO_3$ concentration. Within the study of the Donnan effect, it was found that the influence of NO_3^- coions on TiO_2 NT surfaces is negligible at high pH because a strong electric field repels them from the TiO_2 NT surface. When the pH is close to the pH_{pzc}, the screening becomes inefficient and there is a pronounced penetration of NO_3^- coions into the interior of the TiO_2 NTs.

Currently, the modifications of ion−ion and ion-TiO_2 NT wall interactions are made through the addition of various potentials within the framework of the classical density functional theory.

APPENDIX

In the Theory section, we identified surface groups made of oxygen (O atom) covalently bonded to the titanium atom. The O atom can associate with the proton from the reservoir. The maximum number of protons that can be associated with the O atom (adsorbed to the surface site in the terminology of colloid chemistry) is determined by the accessible volume for protons. Allowing the successive two-step protonation of the site written as

$$\equiv TiO^{-4/3} + H^+ \rightleftharpoons \equiv TiOH^{-1/3} \tag{33}$$

and

$$\equiv TiOH^{-1/3} + H^+ \rightleftharpoons \equiv TiOH_2^{+2/3} \tag{34}$$

the fully deprotonated O atom (corresponding to the $\equiv TiO^{-4/3}$ surface group) therefore has accessible volume two times that of the O atom with already bonded one proton (corresponding to the $\equiv TiOH^{-1/3}$ surface group). The statistical mechanics derivation already reported by our group justifies the use of following expression for the definition of association constant $K^\circ_{H,1}$ between ions.[49]

$$K^\circ_{H,1} = \int_{V_{site,l}} e^{-\beta U(\mathbf{r})}\, d^3r \tag{35}$$

where $K^\circ_{H,1}$ represents protonation constants, $V_{site,l}$ represents volume of sites accessible to protons, index l denotes the type of the surface group, $\beta = 1/k_BT$ and $U(\mathbf{r})$ are the interaction potential for a paired anion and cation (O−H), respectively. We treat protonated surface groups like contact ion pairs. The center of the O atom has been chosen as a center of the coordination system, with R_{O-H} being the distance between the O atom and the associated proton. For the purposes of simplicity, we ignore any change of Ti−O and O−H bond lengths upon the association of the proton (or any other structural change). This is important to emphasize because it simplifies the calculation. Upon division of two protonation constants, the short-ranged part of potential cancels and only the Coulomb part remains. This works because we are only interested in the O−H bond. Therefore, the interaction potential $U(\mathbf{r})$ between the pair is considered to be of Coulombic nature only and can be written as

$$U(\mathbf{r}) = \frac{z_{site,l} e^2}{4\pi\varepsilon_0\varepsilon_{r,1} R_{O-H}} \tag{36}$$

where $z_{site,l}$ is the charge of site l. Dividing the two protonation constants yields

$$\frac{K^\circ_{H,1}}{K^\circ_{H,2}} = \frac{\int_{V_{site,1}} e^{-\beta U(r)}\, d^3r}{\int_{V_{site,2}} e^{-\beta U(r)}\, d^3r} \tag{37}$$

DOI: 10.1021/acsami.7b18737
ACS Appl. Mater. Interfaces XXXX, XXX, XXX−XXX

We have already stated that R_{O-H} does not change, so the two integrals on the right side can be factorized. We obtain

$$\frac{K^{\circ}_{H,1}}{K^{\circ}_{H,2}} = \frac{e^{-\beta z_{site,1} e^2/4\pi\varepsilon_0\varepsilon_{r,1}R_{O-H}}}{e^{-\beta z_{site,2} e^2/4\pi\varepsilon_0\varepsilon_{r,1}R_{O-H}}} \frac{\int_{V_{site,1}} d^3r}{\int_{V_{site,2}} d^3r} \quad (38)$$

Writing the $U(\mathbf{r})$ in terms of Bjerrum length l_B, we have

$$\frac{K^{\circ}_{H,1}}{K^{\circ}_{H,2}} = \frac{e^{-\beta z_{site,1} l_B/R_{O-H}}}{e^{-\beta z_{site,2} l_B/R_{O-H}}} \frac{\int_{V_{site,1}} d^3r}{\int_{V_{site,2}} d^3r} \quad (39)$$

Note that we did not specify the type of the coordinate system. The important fact is that radii vectors describing positions of both particles have the same origin. Taking the natural logarithm of the expression above yields

$$\ln\left(\frac{K^{\circ}_{H,1}}{K^{\circ}_{H,2}}\right) = \frac{l_B(z_{site,2} - z_{site,1})}{R_{O-H}} + \ln\left(\frac{\int_{V_{site,1}} d^3r}{\int_{V_{site,2}} d^3r}\right) \quad (40)$$

The second term is a ratio of accessible volumes for the proton. It is assumed to be equal to ln 2 because we are investigating the two successive protonations (the fully deprotonated surface group $\equiv TiO^{-4/3}$ has twice as much volume for proton, compared to the $\equiv TiOH^{-1/3}$ group). After rearrangement of the former expression, we obtain the value of the O−H bond.

$$R_{O-H} = \frac{l_B(z_{site,2} - z_{site,1})}{\ln\left(\frac{K^{\circ}_{H,1}}{K^{\circ}_{H,2}}\right) - \ln 2} \quad (41)$$

Performing a simple calculation to determine the R_{O-H} values for the sets of intrinsic protonation constants obtained from the fitting procedure yields

$$R_{O-H}(\log K_{H,1} = 4.5,\ \log K_{H,2} = 3) = 2.5\ \text{Å}$$

$$R_{O-H}(\log K_{H,1} = 8.1,\ \log K_{H,2} = 3) = 0.63\ \text{Å}$$

$$R_{O-H}(\log K_{H,1} = 13,\ \log K_{H,2} = 3) = 0.31\ \text{Å}$$

The set of intrinsic protonation constants $\log K_{H,1} = 8.1$ and $\log K_{H,2} = 3$ yields the length of the O−H bond equal to 0.63 Å.

■ ASSOCIATED CONTENT

Supporting Information

The Supporting Information is available free of charge on the ACS Publications website at DOI: 10.1021/acsami.7b18737.

Charge properties of TiO_2 nanotubes in $NaNO_3$ aqueous solution: theory and experiments. Influence of a dielectric constant ϵ_r^2 through TiO_2 layer screening of the inner TiO_2NTs surface charge as a function of the pH large figure of an agglomerate of TiO_2NTs (PDF)

■ AUTHOR INFORMATION

Corresponding Author

*E-mail: bohinck@zf.uni-lj.si.

ORCID

Mario Špadina: 0000-0002-8292-5765
Simon Gourdin-Bertin: 0000-0001-9630-3994
Atiđa Selmani: 0000-0002-5830-2138
Klemen Bohinc: 0000-0003-2126-8762

Notes

The authors declare no competing financial interest.

■ ACKNOWLEDGMENTS

The research leading to these results has received funding from the European Research Council under the European Union's Seventh Framework Programme (FP/2007-2013)/ERC Grant Agreement no. [320915] "REE-CYCLE": Rare Earth Element reCYCling with Low harmful Emissions. The authors thank the Research Agency for support through grant BI-FR/CEA/16-18-002 and the Slovenian Research Agency for support through program P3-0388. The authors thank B. Siboulet and T. Zemb for useful discussions, to R. Fink for the assistance in using PCD, and Aurelio Barbetta for the software technical support.

■ REFERENCES

(1) Kordás, K.; Mohl, M.; Kónya, Z.; Kukovecz, Á. Layered titanate nanostructures: perspectives for industrial exploitation. *Transl. Mater. Res.* **2015**, *2*, 015003.

(2) Liu, W.; Sun, W.; Han, Y.; Ahmad, M.; Ni, J. Adsorption of Cu(II) and Cd(II) on titanate nanomaterials synthesized via hydrothermal method under different NaOH concentrations: Role of sodium content. *Colloids Surf., A* **2014**, *452*, 138−147.

(3) Grover, I. S.; Singh, S.; Pal, B. The preparation, surface structure, zeta potential, surface charge density and photocatalytic activity of TiO2 nanostructures of different shapes. *Appl. Surf. Sci.* **2013**, *280*, 366−372.

(4) Roy, P.; Berger, S.; Schmuki, P. TiO2 nanotubes: Synthesis and applications. *Angew. Chem., Int. Ed.* **2011**, *50*, 2904−2939.

(5) Faria, H. A. M.; de Queiroz, A. A. A. A novel drug delivery of 5-fluorouracil device based on TiO2/ZnS nanotubes. *Mater. Sci. Eng., C* **2015**, *56*, 260−268.

(6) Yang, W.-W.; Wang, Y.; Huang, B.; Wang, N.-X.; Wei, Z.-B.; Luo, J.; Miao, A.-J.; Yang, L.-Y. TiO2 Nanoparticles Act As a Carrier of Cd Bioaccumulation in the Ciliate Tetrahymena thermophila. *Environ. Sci. Technol.* **2014**, *48*, 7568−7575.

(7) Kasuga, T.; Hiramatsu, M.; Hoson, A.; Sekino, T.; Niihara, K. Formation of Titanium Oxide Nanotube. *Langmuir* **1998**, *14*, 3160−3163.

(8) Armstrong, G.; Armstrong, A. R.; Canales, J.; Bruce, P. G. Nanotubes with the TiO2-B structure. *Chem. Commun.* **2005**, 2454−2456.

(9) Patzke, G. R.; Krumeich, F.; Nesper, R. Oxidic nanotubes and nanorods - Anisotropic modules for a future nanotechnology. *Angew. Chem., Int. Ed.* **2002**, *41*, 2446−2461.

(10) Selmani, A.; Špadina, M.; Plodinec, M.; Marion, I. D.; Willinger, M. G.; Lützenkirchen, J.; Gafney, H. D.; Redel, E. An Experimental and Theoretical Approach to Understanding the Surface Properties of One-Dimensional TiO2 Nanomaterials. *J. Phys. Chem. C* **2016**, *120*, 4150.

(11) Bérubé, Y. G.; De Bruyn, P. L. Adsorption at the rutile-solution interface. *J. Colloid Interface Sci.* **1968**, *28*, 92−105.

(12) Bourikas, K.; Vakros, J.; Kordulis, C.; Lycourghiotis, A. Potentiometric Mass Titrations: Experimental and Theoretical Establishment of a New Technique for Determining the Point of Zero Charge (PZC) of Metal (Hydr) Oxides. *J. Phys. Chem. B* **2003**, *107*, 9441−9451.

(13) Hunter, R. J. *Zeta Potential Colloid Science*, 1st ed.; Academic Press, 1981.

(14) Buchhammer, H.-M.; Kramer, G.; Lunkwitz, K. Interaction of colloidal dispersions of non-stoichiometric polyelectrolyte complexes and silica particles. *Colloids Surf., A* **1995**, *95*, 299−304.

(15) Mikkelsen, L. H. Applications and limitations of the colloid titration method for measuring activated sludge surface charges. *Water Res.* **2003**, *37*, 2458−2466.

DOI: 10.1021/acsami.7b18737
ACS Appl. Mater. Interfaces XXXX, XXX, XXX−XXX

(16) Horvath, A. E.; Lindström, T.; Laine, J. On the indirect polyelectrolyte titration of cellulosic fibers. Conditions for charge stoichiometry and comparison with ESCA. *Langmuir* **2006**, *22*, 824−830.
(17) Kam, S.-K.; Gregory, J. Charge determination of synthetic cationic polyelectrolytes by colloid titration. *Colloids Surf., A* **1999**, *159*, 165−179.
(18) Trizac, E.; Hansen, J.-P. Wigner-Seitz model of charged lamellar colloidal dispersions. *Phys. Rev. E: Stat. Phys., Plasmas, Fluids, Relat. Interdiscip. Top.* **1997**, *56*, 3137.
(19) Trefalt, G.; Behrens, S. H.; Borkovec, M. Charge Regulation in the Electrical Double Layer: Ion Adsorption and Surface Interactions. *Langmuir* **2016**, *32*, 380−400.
(20) Behrens, S. H.; Borkovec, M. Exact Poisson-Boltzmann solution for the interaction of dissimilar charge-regulating surfaces. *Phys. Rev. E: Stat. Phys., Plasmas, Fluids, Relat. Interdiscip. Top.* **1999**, *60*, 7040−7048.
(21) Fleck, C.; Netz, R. R.; von Grünberg, H. H. Poisson-Boltzmann theory for membranes with mobile charged lipids and the pH-dependent interaction of a DNA molecule with a membrane. *Biophys. J.* **2002**, *82*, 76−92.
(22) Adžić, N.; Podgornik, R. Charge regulation in ionic solutions: Thermal fluctuations and Kirkwood-Schumaker interactions. *Phys. Rev. E: Stat., Nonlinear, Soft Matter Phys.* **2015**, *91*, 022715.
(23) Duval, J. F. L.; Merlin, J.; Narayana, P. A. L. Electrostatic interactions between diffuse soft multi-layered (bio)particles: beyond Debye-Hückel approximation and Deryagin formulation. *Phys. Chem. Chem. Phys.* **2011**, *13*, 1037−1053.
(24) González, A.; White, J. A.; Román, F. L.; Velasco, S.; Evans, R. Density Functional Theory for Small Systems: Hard Spheres in a Closed Spherical Cavity. *Phys. Rev. Lett.* **1997**, *79*, 2466−2469.
(25) Bohinc, K.; Bossa, G. V.; May, S. Incorporation of ion and solvent structure into mean-field modeling of the electric double layer. *Adv. Colloid Interface Sci.* **2017**, *249*, 220−233.
(26) Xin, Y.; Zheng, Y.-X.; Yu, Y.-X. Density functional theory study on ion adsorption and electroosmotic flow in a membrane with charged cylindrical pores. *Mol. Phys.* **2015**, *114*, 2328−2336.
(27) Lozada-Cassou, M. Hypernetted Chain Theory for the Distribution of Ions around a Cylindrical Electrode. *J. Phys. Chem.* **1983**, *87*, 3729−3732.
(28) Lee, J. W.; Nilson, R. H.; Templeton, J. A.; Griffiths, S. K.; Kung, A.; Wong, B. M. Comparison of Molecular Dynamics with Classical Density Functional and Poisson Boltzmann Theories of the Electric Double Layer in Nanochannels. *J. Chem. Theory Comput.* **2012**, *8*, 2012−2022.
(29) Hocine, S.; Hartkamp, R.; Siboulet, B.; Duvail, M.; Coasne, B.; Turq, P.; Dufrêche, J.-F. How Ion Condensation Occurs at a Charged Surface: A Molecular Dynamics Investigation of the Stern Layer for Water-Silica Interfaces. *J. Phys. Chem. C* **2016**, *120*, 963−973.
(30) Ninham, B. W.; Parsegian, V. A. Electrostatic potential between surfaces bearing ionizable groups in ionic equilibrium with physiologic saline solution. *J. Theor. Biol.* **1971**, *31*, 405−428.
(31) Hiemstra, T.; Van Riemsdijk, W. H. A Surface Structural Approach to Ion Adsorption: The Charge Distribution (CD) Model. *J. Colloid Interface Sci.* **1996**, *179*, 488−508.
(32) Pauling, L. The Principles Determining the Structure of Complex Ionic Crystals. *J. Am. Chem. Soc.* **1929**, *51*, 1010−1026.
(33) Panagiotou, G. D.; Petsi, T.; Bourikas, K.; Garoufalis, C. S.; Tsevis, A.; Spanos, N.; Kordulis, C.; Lycourghiotis, A. Mapping the surface (hydr)oxo-groups of titanium oxide and its interface with an aqueous solution: The state of the art and a new approach. *Adv. Colloid Interface Sci.* **2008**, *142*, 20−42.
(34) Bourikas, K.; Hiemstra, T.; Van Riemsdijk, W. H. Ion pair formation and primary charging behavior of titanium oxide (anatase and rutile). *Langmuir* **2001**, *17*, 749−756.
(35) Gisler, T.; Schulz, S. F.; Borkovec, M. Understanding colloidal charge renormalization from surface chemistry: Experiment and theory. *J. Chem. Phys.* **1994**, *101*, 9924.
(36) Sverjensky, D. A. Standard states for the activities of mineral surface sites and species. *Geochim. Cosmochim. Acta* **2003**, *67*, 17−28.
(37) Kallay, N.; Preocanin, T.; Kovacevic, D.; Lutzenkirchen, J.; Chibowski, E. Electrostatic Potentials at Solid/Liquid Interfaces. *Croat. Chem. Acta* **2010**, *83*, 357−370.
(38) Van Riemsdijk, W. H.; Bolt, G. H.; Koopal, L. K.; Blaakmeer, J. Electrolyte adsorption on heterogenous surfaces: adsorption models. *J. Colloid Interface Sci.* **1986**, *109*, 219−228.
(39) Hansen, J.-P.; Löwen, H. Effective interaction between electric double-layers. *Annu. Rev. Phys. Chem.* **2000**, *51*, 209−242.
(40) Allaire, G.; Dufrêche, J.-F.; Mikelić, A.; Piatnitski, A. Asymptotic analysis of the Poisson - Boltzmann equation describing electrokinetics in porous media. *Nonlinearity* **2013**, *26*, 881−910.
(41) Smith, D. A.; Ford, W. F. Numerical Comparisons of Nonlinear Convergence Accelerators. *Math. Comput.* **2007**, *38*, 481−499.
(42) Mandzy, N.; Grulke, E.; Druffel, T. Breakage of TiO2 agglomerates in electrostatically stabilized aqueous dispersions. *Powder Technol.* **2005**, *160*, 121−126.
(43) Bavykin, D. V.; Walsh, F. C. Kinetics of Alkali Metal Ion Exchange into Nanotubular and Nanofibrous Titanates. *J. Phys. Chem. C* **2007**, *25*, 14644−14651.
(44) Deserno, M.; Holm, C.; May, S. Fraction of condensed counterions around a charged rod: Comparison of Poisson-Boltzmann theory and computer simulations. *Macromolecules* **2000**, *33*, 199−206.
(45) Pelton, R.; Cabane, B.; Cui, Y.; Ketelson, H. Shapes of polyelectrolyte titration curves. 1. Well-behaved strong polyelectrolytes. *Anal. Chem.* **2007**, *79*, 8114−8117.
(46) Böckenhoff, K.; Fischer, W. R. Determination of electrokinetic charge with a particle-charge detector, and its relationship to the total charge. *Fresenius. J. Anal. Chem.* **2001**, *371*, 670−674.
(47) Dzombak, D. A.; Morel, F. M. M. *Surface Complexation Modeling: Hydrous Ferric Oxide*; John Wiley & Sons Ltd: New York, 1990.
(48) Hiemstra, T.; Van Riemsdijk, W. H.; Bolt, G. H. Multisite proton adsorption modeling at the solid/solution interface of (hydr) oxides: A new approach: I. Model description and evaluation of intrinsic reaction constants. *J. Colloid Interface Sci.* **1989**, *133*, 91−104.
(49) Molina, J. J.; Dufrêche, J.-F.; Salanne, M.; Bernard, O.; Turq, P. Primitive models of ions in solution from molecular descriptions: A perturbation approach. *J. Chem. Phys.* **2011**, *135*, 234509.
(50) Molina, J. J.; Dufrêche, J.-F.; Salanne, M.; Bernard, O.; Jardat, M.; Turq, P. Models of electrolyte solutions from molecular descriptions: The example of NaCl solutions. *Phys. Rev. E: Stat. Phys., Plasmas, Fluids, Relat. Interdiscip. Top.* **2009**, *80*, 65103.
(51) Siboulet, B.; Hocine, S.; Hartkamp, R.; Dufrêche, J.-F. Scrutinizing Electro-Osmosis and Surface Conductivity with Molecular Dynamics. *J. Phys. Chem. C* **2017**, *121*, 6756−6769.
(52) Wang, R.; Wang, Z.-G. On the theoretical description of weakly charged surfaces. *J. Chem. Phys.* **2015**, *142*, 104705.
(53) Schwierz, N.; Netz, R. R. Effective interaction between two ion-adsorbing plates: Hofmeister series and salting-in/salting-out phase diagrams from a global mean-field analysis. *Langmuir* **2012**, *28*, 3881−3886.
(54) Colla, T.; Girotto, M.; dos Santos, A. P.; Levin, Y. Charge neutrality breakdown in confined aqueous electrolytes: Theory and simulation. *J. Chem. Phys.* **2016**, *145*, 094704.
(55) Holmberg, J. P.; Ahlberg, E.; Bergenholtz, J.; Hassellöv, M.; Abbas, Z. Surface charge and interfacial potential of titanium dioxide nanoparticles: Experimental and theoretical investigations. *J. Colloid Interface Sci.* **2013**, *407*, 168−176.
(56) Schwierz, N.; Horinek, D.; Sivan, U.; Netz, R. R. Reversed Hofmeister series - The rule rather than the exception. *Curr. Opin. Colloid Interface Sci.* **2016**, *23*, 10−18.

DOI: 10.1021/acsami.7b18737
ACS Appl. Mater. Interfaces XXXX, XXX, XXX−XXX